X-ray Raman scattering provides evidence for interfacial acetonitrile-water dipole interactions in aqueous solutions

Ningdong Huang,[1] Dennis Nordlund,[1] Congcong Huang,[1] Uwe Bergmann,[1] Thomas M. Weiss,[1] Lars G. M. Pettersson,[2] and Anders Nilsson[1,2,a)]
[1]*Stanford Synchrotron Radiation Lightsource, P.O.B. 20450, Stanford, California 94309, USA*
[2]*Department of Physics, AlbaNova, Stockholm University, S-106 91 Stockholm, Sweden*

(Received 26 May 2011; accepted 4 October 2011; published online 28 October 2011)

Aqueous solutions of acetonitrile (MeCN) have been studied with oxygen K-edge x-ray Raman scattering (XRS) which is found to be sensitive to the interaction between water and MeCN. The changes in the XRS spectra can be attributed to water directly interacting with MeCN and are reproduced by density functional theory calculations on small clusters of water and MeCN. The dominant structural arrangement features dipole interaction instead of H-bonds between the two species as revealed by the XRS spectra combined with spectrum calculations. Small-angle x-ray scattering shows the largest heterogeneity for a MeCN to water ratio of 0.4 in agreement with earlier small-angle neutron scattering data. © *2011 American Institute of Physics*. [doi:10.1063/1.3655468]

I. INTRODUCTION

Water and acetonitrile (MeCN) can be mixed at any ratio and the aqueous solutions are widely used in many fields such as liquid chromatography, solvent extraction, organic synthesis, and electrochemistry. Three composition regions, which can be characterized by different structural patterns, have been established by many methods.[1–3] In the first, water-rich region ($0 < X_{\mathrm{MeCN}} < 0.2$), the acetonitrile molecules occupy cavities in the water network without disturbing the water structure. With an increase of the acetonitrile concentration ($0.2 < X_{\mathrm{MeCN}} < 0.75$) the water structure undergoes a gradual disruption and clusters are formed. The third region ($X_{\mathrm{MeCN}} > 0.75$) can be visualized as an acetonitrile arrangement disturbed by water molecules forming small water clusters rather than a continuous H-bond network.

In addition, microscopic heterogeneity or coexistence of clusters of the two species in the solution is also confirmed by experiments[2–4] as well as by molecular dynamics simulations.[5] The mechanism of inhomogeneous mixing in the MeCN-water binary system can be understood through a variety of interactions with different strengths and origin in the mixture.[6] MeCN molecules aggregate through dipole-dipole interactions while water molecules form hydrogen bonds (H-bonds) among each other. In aqueous solution two different types of interacting configurations between water and MeCN have been proposed where the OH axis of water and the CN axis of MeCN are either in-line, forming a H-bond between the hydrogen and the nitrile nitrogen, or in side-by-side antidipole arrangement with the CN bond parallel to the plane of the water molecule.[7,8] In either configuration, inter-species interactions will be weaker than that between water molecules; consequently, water molecules aggregate with themselves and so do MeCN molecules. Both types of MeCN-water configurations have been observed at interfaces or on surfaces,[9,10] but in aqueous solution most existing experiments cannot distinguish the two configurations and are conventionally interpreted based on H-bonds between water and MeCN.

X-ray absorption spectroscopy (XAS) and the corresponding hard x-ray energy loss version x-ray Raman scattering (XRS) have been shown to give a large spectral sensitivity for different hydrogen bonding (H-bond) configurations.[11–19] Although there is a debate on the theoretical description of XAS/XRS (Refs. 20–25) the sensitivity to the change of H-bond topology with temperature, is well established experimentally.[11,12,26] In particular, it can be shown that the pre- (535 eV) and main-edge peaks (537–538 eV) fingerprint distorted H-bonds, whereas the post-edge (540–541 eV) is associated with strong H-bonds and is further enhanced for tetrahedral H-bond structures. This interpretation has been supported by experiments on H-bonded model systems on surfaces.[14] It has also recently been shown that the main-edge intensity gets enhanced upon formation of high density forms of ice such as high-density amorphous ice (HDA) (Ref. 18) and various crystalline high pressure ices such as I_{II}, I_{VI}, I_{VII}, and I_{VIII}.[27]

In the present study, measured and density functional theory (DFT) computed oxygen 1s XAS of water was found to be sensitive to the different types of proposed interaction between the two species with spectral changes in the experiment fairly well reproduced by the spectrum simulations. Careful consideration of the detection scheme for XAS is necessary in order to avoid artifacts with respect to quantitative aspects of the spectral features as discussed in references.[11,28] Here we use XRS for its sample environment advantages (bulk sensitivity and ambient pressure) and high reliability regarding the relative intensities of spectral features. The discrepancy between the present XRS measurements and a recent XAS study on the same system[29] using fluorescence yield (FY) detection will be further discussed.

a)Author to whom correspondence should be addressed. Electronic mail: nilsson@slac.stanford.edu.

II. METHODS

The solutions were made from distilled water and pure chemicals purchased from Sigma Aldrich with no further purification.

The small-angle x-ray scattering (SAXS) experiments were performed at beamline 4–2 at the Stanford Synchrotron Radiation Lightsource (SSRL) using beam energy of 11 keV and an optical fiber coupled CCD detector (Rayonix225HE). A quartz capillary with an inner diameter of 1.5 mm was integrated into a sample cooling holder kept in a nitrogen gas atmosphere to eliminate water condensation. The scattering momentum transfer Q is defined as $Q = 4\pi \sin\theta/\lambda$, with λ the wavelength and θ one half of the scattering angle. To reduce the possibility of radiation damage, the data were continuously collected for 10 frames with 1 min each and all scattering images were averaged afterward. The scattering curves have been corrected for the primary beam intensity, absorption and detector readout noise.

XRS measurements were performed at beamline 6–2 at the SSRL using a Si(311) double crystal monochromator. Raman scattering at ~45° (in the horizontal plane) is analyzed with a high-resolution multi-crystal spectrometer analyzer consisting of 14 Si(440) analyzer crystals with a diameter of 100 mm on intersecting Rowland circles (1 m radius) operated close to backscattering at a Bragg angle of 88° (in the vertical plane), and an energy of 6.46 keV. The corresponding momentum transfer is $q = 2.5 \pm 1$ Å^{-1} with $qr = 0.1 \sim 0.23$ for Oxygen 1s XRS which is small enough that dipole transitions strongly dominate. The Raman spectrum is obtained by scanning the beamline monochromator energy at a fixed analyzer setting (6.46 keV), and the energy difference (beamline monochromator energy minus analyzer energy) corresponds to the energy range around the oxygen K-edge; note that since XRS is a non-resonant technique there is no excitation energy dependence. The overall energy resolution (convolution of beamline and analyzer resolution) is found to be 0.55 ± 0.1 eV full width at half maximum (FWHM) through measurements of the elastic scattering peak. The scattered intensity is measured by a Vortex single-element Si drift detector in photon counting mode with an electronic window centered around 6.46 keV, set to reduce the background signal. The detector intensity was normalized to the incoming photon flux, recorded with a He filled ion chamber. The Raman spectrum is furthermore corrected for background (dominated by Compton scattering) by subtracting a linear background fitted to the region well below the absorption edge.

Spectrum calculations were performed using the StoBeDeMon DFT program[30] with the transition-potential half-core-hole approach.[20,31] The core-excited atom, placed in the center of the cluster, is described using the IGLO-III all-electron basis set,[32] allowing for the relaxation of the core-hole, while all other (C, N, O) atoms are described by an effective core potential (ECP) (Ref. 33) and hydrogen is described by the (5s)/[3s] basis of Ref. 34 with one added *p*-function. Replacing the core-level by an ECP for all atoms except the core-excited allows us to safely locate the core-hole on the atom of interest. The discrete oscillator strengths are computed and then convoluted to form the XAS spectrum using Gaussian broadening with constant FWHM of 1 eV below 537 eV then linearly increased up to 3 eV at 545 eV and remaining constant afterward at higher energy. This approach is used to mimic the experimental broadening of the transitions which has instrumental, vibrational as well as life-time origin. The excitation energy is computed with the ΔKohn–Sham method where the spectrum onset is obtained as the energy difference between the ground state and the first core-excited state.[35] A relativistic energy shift of 0.33 eV is also included.[36]

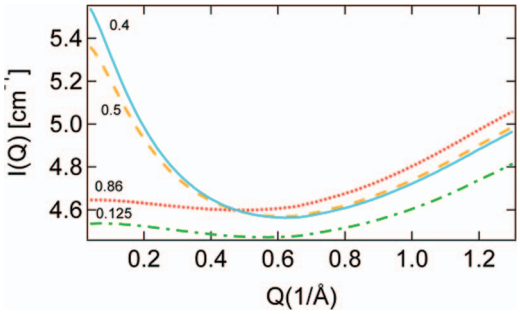

FIG. 1. SAXS intensity of MeCN aqueous solutions versus momentum transfer. The numbers give the MeCN mole fraction.

III. RESULTS AND DISCUSSION

The character of the micro-heterogeneous mixing of water and MeCN is first investigated through SAXS with results given in Fig. 1. The enhancement at low Q in the SAXS is due to heterogeneities arising either through fluctuations in the local concentration of species in the solution or through local microsegregation between species. A big jump in the low-Q signal is observed upon going from the water rich ($X_{\mathrm{MeCN}} = 0.125$) region to intermediate mixture ($X_{\mathrm{MeCN}} = 0.4$) in which case microscopic domains of the different molecules are formed in the solution. The low-Q SAXS intensity is then observed to decrease at higher X_{MeCN} and is even suppressed at $X_{\mathrm{MeCN}} = 0.86$ when only very small water clusters are present in the sea of MeCN molecules.[3,4] The SAXS signal in Fig. 1 thus shows the largest enhancement around $X_{\mathrm{MeCN}} = 0.4$ consistent with a previous small-angle neutron scattering study where the heterogeneity was found to be most enhanced at $X_{\mathrm{MeCN}} = 0.3$ and 0.4.[4,37]

Measured XRS spectra at various concentrations are shown in Fig. 2. (Note that in all figures of experimental data, the labels "X-ray Photon Energy" correspond to the energy transfer in the XRS process.) It has been demonstrated that the pre- (535 eV) and main-edge peaks (537–538 eV) fingerprint distorted H-bonds, whereas the post-edge (540–541 eV) is associated with strong H-bonds and is further enhanced for tetrahedral H-bond structures.[11,12,38] In the first concentration range with $X_{\mathrm{MeCN}} = 0.1$, O 1s XRS shows evidence for weaker hydrogen bonding (H-bonding) structure of water, as manifested by the reduced post-edge intensity, while the pre- and main-edges are enhanced. At this low concentration, the picture derived from other experiments and simulations is that almost all MeCN molecules are engaged in interaction

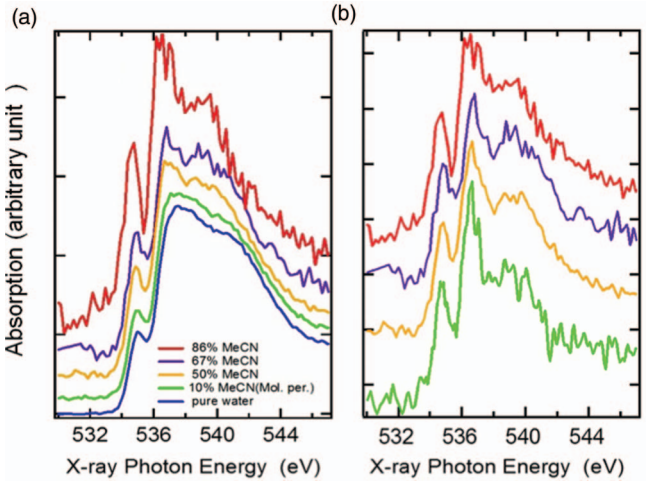

FIG. 2. XRS spectra normalized to the spectral area between 531 and 545 eV of (a) aqueous MeCN solutions with concentration of MeCN increasing from bottom to top and (b) water interacting with MeCN obtained by subtracting the estimated pure water-like contribution to each spectrum as described in the text. The percentage pure water contribution is estimated to be 90%, 60%, and 50% for $X_{\mathrm{MeCN}} = 0.1$, 0.5, and 0.6, respectively. Those numbers are approximate but the shape of the resulting difference spectra is found to not be very sensitive to the ratio used in the subtraction procedure.

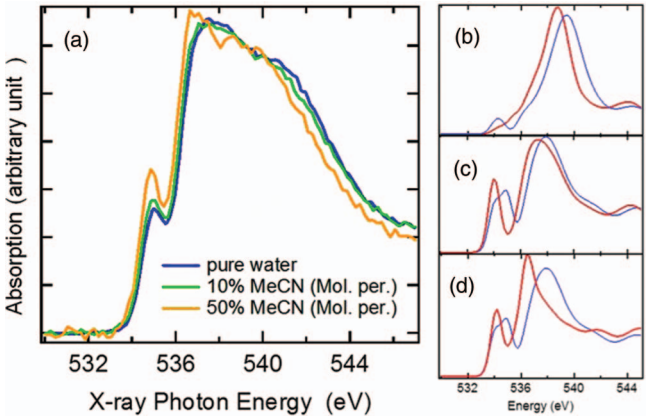

FIG. 3. Energy shifts of the absorption edges in XAS observed by experiments and simulation. (a) Experimental spectra of MeCN aqueous solutions in comparison with pure water. (b) DFT calculations with the central water molecule donating two H-bonds to two water (blue curve on the right) or MeCN (red curve on the left) molecules, showing shift of the post-edge feature. (c) DFT calculations of the central water molecule donating only one H-bond to another water (blue curve on the right) in comparison to water bonded to one MeCN (red curve on the left), showing the shift and enhancement in pre- and main edges. (d) Water and MeCN in dipole interacting structural arrangement (red curve on the left) compared to the central water molecule donating only one H-bond to another water (blue curve on the right, from c). The geometry and coordination of the clusters are adapted from optimized structures in the literature.[7,39]

with surrounding water. The XRS spectral changes are probably dominated by the direct interaction of water with MeCN as will be discussed later. As the fraction of MeCN increases to 50%, the intensity at the pre- and main-edge continues to increase and the peak positions are shifted to lower energies, indicating further distortions in the H-bond structure of water. The spectra remain bulk-like but new features appear, such as the shift of the post-edge to lower energy between 538 and 540 eV compared to 541 eV for pure water; these features become further enhanced in the spectrum for a higher concentration of $X_{\mathrm{MeCN}} = 67\%$. In the MeCN rich concentration range of $X_{\mathrm{MeCN}} = 86\%$, the spectrum differs strongly from that of liquid water and shows much sharper pre-, main-, and post-edge features which are, however, shifted to lower energy compared to pure water. The pre- and main-edge peaks resemble the discrete peaks for gas phase, but are located at somewhat higher energy; the post-edge located below 540 eV is unique for MeCN-water. It will be demonstrated through DFT calculations that the position of the post-edge is a result of the longer H-bond length associated with H-bonds formed between water and MeCN.

Based on the micro-heterogeneity in the solution as mentioned in the introduction and demonstrated through the SAXS measurements in Fig. 1, we assumed that only water molecules interacting with MeCN contribute to the XRS spectral changes while those residing inside water domains remain bulk-like. The fraction of MeCN interacting with water has been estimated in the literature at various concentrations[2,5] and thus the contribution to the spectra from those water molecules can be derived by subtracting from the spectra of the solutions the contribution from water interacting only with water represented as the spectrum of pure liquid water multiplied by the fraction of such water molecules. The resulting difference spectra given in Fig. 2(b) show little concentration dependence, even in the dilute case of $X_{\mathrm{MeCN}} = 10\%$ where the difference spectrum is the most noisy due to the 90% pure water background subtraction. Moreover, the difference spectra at low concentrations share many common features with the spectrum at highest concentration of $X_{\mathrm{MeCN}} = 0.86$ in which case all water molecules are engaged in interaction with MeCN.[2,5] The fact that the difference spectra are similar at all concentrations indicates that the changes in solutions compared to pure water indeed are due to the interaction between MeCN and water at the interface of microdomains in the mixture.

The experimentally observed spectral changes can be better understood through DFT spectrum simulations based on different local structures of small water-MeCN complexes modeling the interaction between MeCN and water. In Fig. 3(a), experimental XRS spectra at selected concentrations of MeCN are plotted together to emphasize the spectral changes which are qualitatively demonstrated by the simulated spectra in Figs. 3(b)–3(d). Figure 3(b) shows computed spectra of a central water molecule donating two H-bonds to either two water (blue curve on the right) or two MeCN (red curve on the left) with O–O and O–N distance 2.8 Å (Ref. 39) and 3 Å,[7] respectively. Both configurations in Fig. 3(b) show a single sharp peak at high energy corresponding to the post-edge in the solution which is consistent with the assignment of the post-edge feature as being associated with donated H-bonds; water molecules donating both hydrogens then give the largest contribution.[11,12,38] Moreover, it can be seen that the peak position for the water-MeCN cluster in the solution shifts by about 1 eV to lower energy compared to that for the water-water cluster in pure water, which is fully consistent with experiment (Fig. 3(a)). According to the bond length with a ruler concept,[40] the position of the post-edge depends on the bond length or, equivalently, the O–O (O–N)

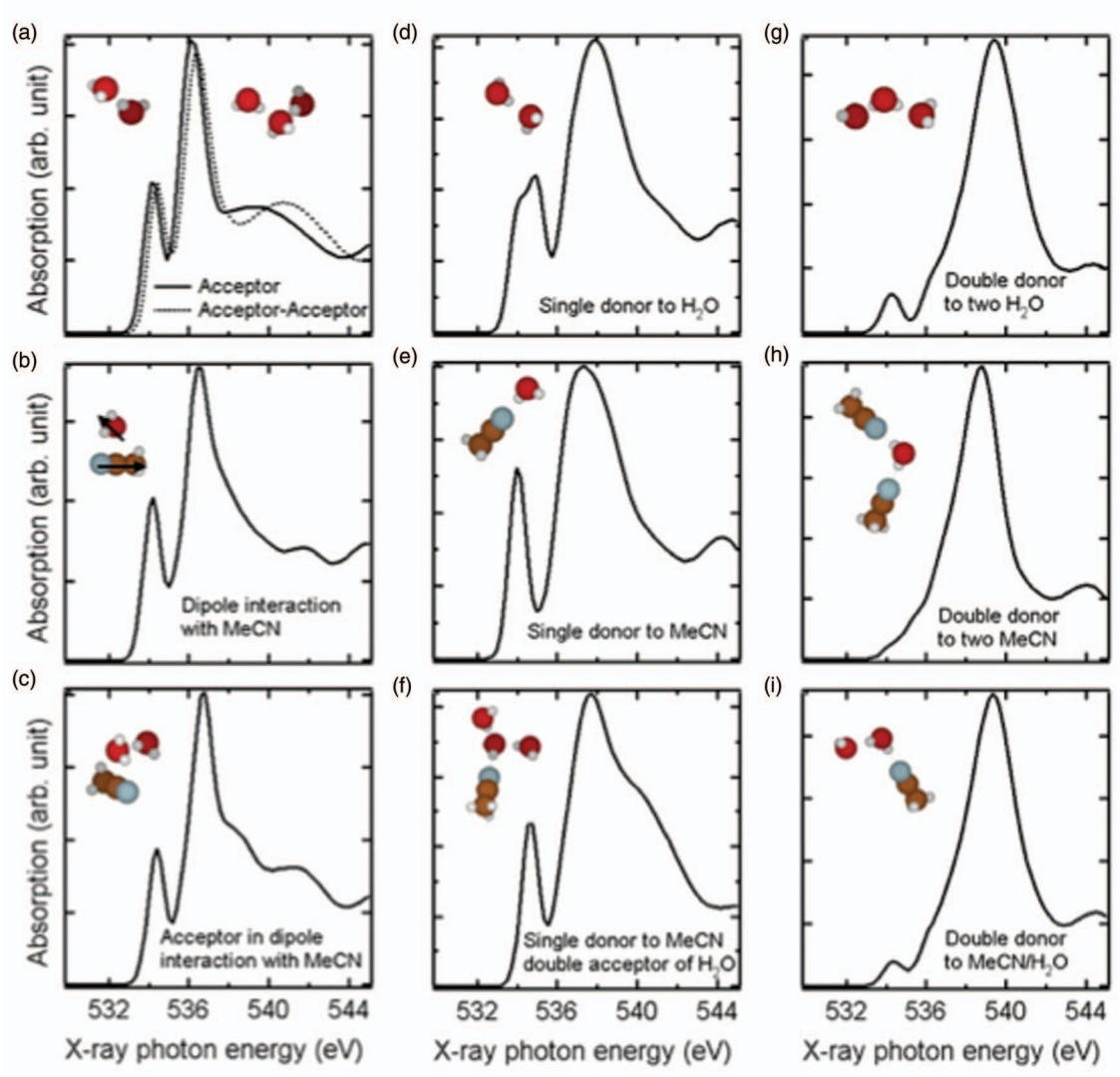

FIG. 4. Summary of donating configurations of water in aqueous MeCN solution. The left three panels are examples of nondonor species where the central water molecule has two dangling OH groups leading to spectra resembling gas phase, including (a) water accepting one (full line) or two (dotted line) H-bonds; (b) water in dipole interaction with MeCN and (c) water accepting one H-bond while in dipole interaction with MeCN. The middle three panels show possible configurations for single-donor species with one dangling OH group and the other (d) donated to water or (e) to MeCN. Panel (f) illustrates the effects on the simulated spectrum from accepting two H-bonds in the configuration in (e). The three panels in right-hand side belong to double-donor species where the two H-bonds are donated to two water molecules in (g), or to two MeCN molecules in (h), or to one water and one MeCN in (i).

distance between molecules.[11,13,41] Hence the energy shift of the post-edge to lower energy can be understood through H-bond formation between water and MeCN at longer H-bond distance than for water H-bonding to water.

The pre- and main-edge features are simulated through models where water molecules either donate only one H-bond to another molecule or water is in dipole interaction with MeCN. The spectrum of the donor in a water-water H-bond (blue curve on the right in Figs. 3(c) and 3(d)) is compared to that of water donating a H-bond to MeCN (red curve on the left) in Fig. 3(c) or in dipole interaction with MeCN in Fig. 3(d); both water-MeCN configurations give sharper pre- and main-edge peaks shifted to lower energy compared to the single-donor water-water configuration. On a qualitative level, such peak shifts are in good agreement with experiment (Fig. 3(a)) and can be understood as a result of the weaker interaction between the two species, both in terms of H-bonding and dipole interaction, compared to formation of water-water H-bonds.

A quantitative analysis of the experimental changes is achieved by fitting the difference spectra in Fig. 2(b) with calculated spectra of small water clusters representing different chemical environments for water, or more specifically the donating configuration of water molecules in the solution. Figure 4 gives several examples of possible configurations for a central water molecule which can be categorized into three classes according to the spectral shape. Linear combinations of calculated spectra of the three classes are used to fit the experimental difference spectra in Fig. 2(b), as depicted in Fig. 5.

The first type of donating configuration is the nondonor type water, with two non-H-bonded hydrogens, interacting with other molecules by accepting H-bonds (Fig. 4(a)) or through dipole interaction with MeCN (Fig. 4(b)) or both

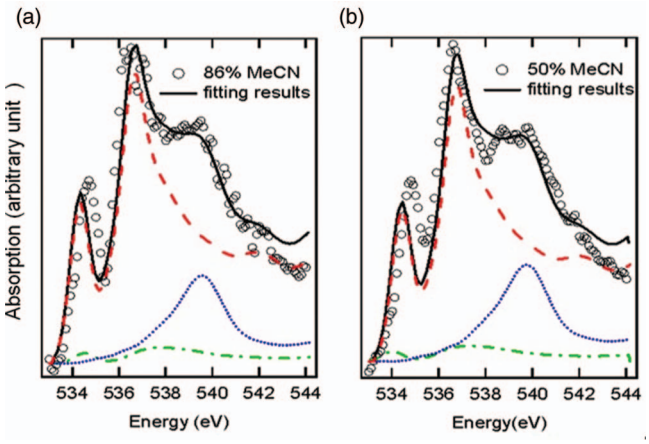

FIG. 5. Fitting experimental spectra of (a) $X_{MeCN} = 0.86$ and (b) $X_{MeCN} = 0.5$ after subtraction of pure water background (with a factor of 0.6 estimated to be the ratio of pure water) using simulated spectra of different donating configurations adapted from Fig. 4. Open circles are experimental data and full lines are results of the fit. The simulated spectra for non-donor (water-MeCN in dipole arrangement), single-donor (water donating to one MeCN) and double-donor (water donating to two MeCN) are denoted by red dashed, green dashed–dotted, and blue dotted line, respectively. The parameters used for fitting are given in Tables I and II.

(Fig. 4(c)). The contribution to the XRS of such water molecules is characterized by features very similar to gas phase but shifted to higher energy,[21] implying that the unoccupied orbitals of the non-donor are only slightly affected compared to gas phase. Another type of structure consists of water donating only one H-bond to another water (Fig. 4(d)) or to MeCN (Fig. 4(e)). Because of the asymmetric H-bond configuration, this type also shows a sharp peak at the pre-edge region and other features similar to those of the non-donor; however, those features are of different natures for the non-donor and single-donor species. The difference is mainly reflected in the main-edge peak which is broadened and shifted to higher energy in the single-donor configuration in comparison to the nondonor case. The H-bond configuration on the accepting side only induces slight changes in the shape of the spectrum as demonstrated in Fig. 4(f) where the central single-donor water molecule also accepts two H-bonds. When both hydrogen atoms are donated, as in double-donor configurations, a dominant peak in the post-edge region at higher energy is observed for all possible acceptor configurations as demonstrated in Figs. 4(g)–4(i).

Figure 5 shows the best-fit spectra of water-MeCN interaction derived from experimental data in Fig. 2(b) in terms of a linear combination of calculated spectra of nondonor (Fig. 4(b)), single-donor (Fig. 4(e)), and double-donor species (Fig. 4(h)). The fitting parameters are given in Tables I and II

TABLE I. Parameters used to fit the spectrum of 86% MeCN (Fig. 5(a)). The numbers used in Fig. 5(a) are listed as best fit and the variation ranges of parameters for reasonable fitting are also given here.

Fitting parameters		Single donor	Double donor	Nondonor
Energy shift	Best fit	0.5	0.8	0.15
	Variation	0–0.5	0.5–1.0	0.12–0.17
Percent by area	Best fit	5	18	77
	Variation	0–15	15–20	70–80

TABLE II. Parameters used to fit the spectrum of 50% MeCN in Fig. 5(b).

Fitting parameters		Single donor	Double donor	Nondonor
Energy shift	Best fit	0	1.0	0.25
	Variation	0–0.5	0.8–1.2	0.25–0.27
Percent by area	Best fit	5	20	75
	Variation	0–15	19–21	66–80

for two selected concentrations. A good fit of the pre- and main-edge is found to require a major contribution from the nondonor species, about 75% for both concentrations in Fig. 5, which is already evident in the sharp peaks similar to the gas phase spectrum. It implies that at all concentrations of MeCN aqueous solutions a majority of the water molecules interacting with MeCN exist with two non-H-bonded OH-groups. Our finding is consistent with a previous simulation showing that MeCN molecules orient parallel to the water interface instead of forming H-bonds with the dangling OH groups present at the interface between water and MeCN in a microheterogeneous mixture.[42] Without donating H-bonds, water molecules could instead lower their chemical potential through dipole interaction with MeCN in aqueous solutions. Even water monomers isolated from other water molecules can be similarly stabilized in the solution at very high concentration of MeCN. This explains the appearance of a sharp spectral feature corresponding to water monomers in IR measurements of the OD stretch mode of HDO and CD_3CN as the concentration of water decreases.[3] In comparison, neither wide-angle x-ray diffraction[37] nor neutron diffraction[43] can distinguish between dipole-dipole and H-bonding interactions in MeCN solutions.

A recent study[29] on aqueous solutions of MeCN using XAS measured by FY reported spectral features quite different from the XRS spectra reported here. In particular, the post-edge intensity in the XAS spectra exceeded all other peaks at all measured concentrations ranging from very dilute to high concentration ($X_{water} \approx 0.67$) of water. This unusual spectral profile, which was interpreted as symmetric H-bonding of water to MeCN, leads to inconsistency, not only with the current study, but also with other experiments such as the IR experiments discussed above.[3] A possible reason is given by the saturation effects in the FY detection scheme[11,28] that are clearly present in spectra of Ref. 29; this is also discussed in detail by those authors, but mainly focusing on the post-edge. We speculate that the XAS FY spectra are modified due to saturation effects more strongly around the main-edge where the cross section is the largest; this is clearly seen in the spectra with higher water concentration in particular for the benzene and chloroform datasets of Ref. 29. For lower concentrations of water, saturation decreases, producing higher pre- and main-edge, which is opposite to what is seen in the present study.

IV. CONCLUSION

Through analysis of XRS spectra of MeCN aqueous solutions at a range of concentrations, we find a predominance at the MeCN-water interface of nondonor water molecules in dipole interaction between water and MeCN.

This is consistent with simulations on solutions which found that MeCN molecules orient parallel to the water interface instead of forming H-bonds to the dangling OH groups present at the interface between water and MeCN in the microheterogeneous mixture.[42] This preferential orientation of MeCN has also been observed in experiments at interfaces of liquid/vapor(gas) and on MeCN interacting with solid water;[8,9,44] the present results however constitute the first experimental observation of this phenomenon in solutions.

ACKNOWLEDGMENTS

This work was supported by the National Science Foundation (US) CHE-0431425 and CHE-0809324 and an ALS doctoral fellowship. This research was carried out in part at SLAC Synchrotron Radiation Lightsource (SSRL), a national user facility operated by Stanford University on behalf of the U.S. Department of Energy, Office of Basic Energy Sciences. The authors also acknowledge the support of the SSRL Structural Molecular Biology group by the National Institutes of Health, National Center for Research Resources, Biomedical Technology Grant and the U.S. Department of Energy, Office of Biological and Environmental Research.

[1] C. Moreau and G. Douhéret, J. Chem. Thermodyn. **8**, 403 (1976).
[2] T. Takamuku, M. Tabata, A. Yamaguchi, J. Nishimoto, M. Kumamoto, H. Wakita, and T. Yamaguchi, J. Phys. Chem. B **102**, 8880 (1998).
[3] D. Jamroz, J. Stangret, and J. Lindgren, J. Am. Chem. Soc. **115**, 6165 (1993).
[4] T. Takamuku, Y. Noguchi, M. Matsugami, H. Iwase, T. Otomo, and M. Nagao, J. Mol. Liq. **136**, 147 (2007).
[5] D. L. Bergman and A. Laaksonen, Phys. Rev. E **58**, 4706 (1998).
[6] K. Nishikawa, Y. Kasahara, and T. Ichioka, J. Phys. Chem. B **106**, 693 (2002).
[7] I. Bakó, T. Megyes, and G. Pálinkás, Chem. Phys. **316**, 235 (2005).
[8] S. Bahr and V. Kempter, J. Chem. Phys. **130**, 214509 (2009).
[9] J. Kim, K. C. Chou, and G. A. Somorjai, J. Phys. Chem. B **107**, 1592 (2003).
[10] D. Zhang, J. Gutow, and K. B. Eisenthal, J. Phys. Chem. **98**, 13729 (1994).
[11] A. Nilsson, D. Nordlund, I. Waluyo, N. Huang, H. Ogasawara, S. Kaya, U. Bergmann, L.-Å. Näslund, H. Öström, Ph. Wernet, K. J. Andersson, T. Schiros, and L. G. M. Pettersson, J. Electron. Spectrosc. Relat. Phenom. **177**, 99 (2010).
[12] Ph. Wernet, D. Nordlund, U. Bergmann, M. Cavalleri, M. Odelius, H. Ogasawara, L. Å. Näslund, T. K. Hirsch, L. Ojamäe, P. Glatzel, L. G. M. Pettersson, and A. Nilsson, Science **304**, 995 (2004).
[13] M. Cavalleri, L.-Å. Näslund, D. C. Edwards, Ph. Wernet, H. Ogasawara, S. Myneni, L. Ojamäe, M. Odelius, A. Nilsson, and L. G. M. Pettersson, J. Chem. Phys. **124**, 194508 (2006).
[14] D. Nordlund, H. Ogasawara, K. J. Andersson, M. Tatarkhanov, M. Salmerón, L. G. M. Pettersson, and A. Nilsson, Phys. Rev. B **80**, 233404 (2009).
[15] I. Waluyo, C. Huang, D. Nordlund, U. Bergmann, T. M. Weiss, L. G. M. Pettersson, and A. Nilsson, J. Chem. Phys **134**, 064513 (2011).
[16] T. Schiros, L.-Å. Näslund, K. Andersson, J. Gyllenpalm, G. S. Karlberg, M. Odelius, H. Ogasawara, L. G. M. Pettersson, and A. Nilsson, J. Phys. Chem. C **111**, 15003 (2007).
[17] T. Schiros, H. Ogasawara, O. Takahashi, H. Öström, K. Andersson, L. G. M. Pettersson, A. Nilsson, S. Haq, and A. Hodgson, Chem. Phys. Lett. **429**, 415 (2006).
[18] J. S. Tse, D. M. Shaw, D. D. Klug, S. Patchkovski, G. Vanko, G. Monaco, and M. Krisch, Phys. Rev. Lett. **100**, 095502 (2008).
[19] T. Pylkkänen, V. M. Giordano, J. C. Chervin, A. Sakko, M. Hakala, J. A. Soininen, K. Hämäläinen, G. Monaco, and S. Huotari, J. Phys. Chem. B **114**, 3804 (2010).
[20] M. Leetmaa, M. P. Ljungberg, A. P. Lyubartsev, A. Nilsson, and L. G. M. Pettersson, J. Electron. Spectrosc. Relat. Phenom. **177**, 135 (2010).
[21] M. Cavalleri, H. Ogasawara, L. G. M. Pettersson, and A. Nilsson, Chem. Phys. Lett. **364**, 363 (2002).
[22] M. Cavalleri, D. Nordlund, M. Odelius, A. Nilsson, and L. G. M. Pettersson, Phys. Chem. Chem. Phys. **7**, 2854 (2005).
[23] M. Iannuzzi, J. Chem. Phys. **128**, 204506 (2008).
[24] D. Prendergast and G. Galli, Phys. Rev. Lett. **96**, 215502 (2006).
[25] W. Chen, X. Wu, and R. Car, Phys. Rev. Lett. **105**, 017802 (2010).
[26] C. Huang, K. T. Wikfeldt, T. Tokushima, D. Nordlund, Y. Harada, U. Bergmann, M. Niebuhr, T. M. Weiss, Y. Horikawa, M. Leetmaa, M. P. Ljungberg, O. Takahashi, A. Lenz, L. Ojamäe, A. P. Lyubartsev, S. Shin, L. G. M. Pettersson, and A. Nilsson, Proc. Natl. Acad. Sci. U.S.A. **106**, 15214 (2009).
[27] A. Nilsson, H. Ogasawara, M. Cavalleri, D. Nordlund, M. Nyberg, Ph. Wernet, and L. G. M. Pettersson, J. Chem. Phys. **122**, 154505 (2005).
[28] L. Å. Näslund, J. Lüning, Y. Ufuktepe, H. Ogasawara, Ph. Wernet, U. Bergmann, L. G. M. Pettersson, and A. Nilsson, J. Phys. Chem. B **109**, 13835 (2005).
[29] K. M. Lange, K. F. Hodeck, U. Schade, and E. F. Aziz, J. Phys. Chem. B **114**, 16997 (2010).
[30] K. Hermann, L. G. M. Pettersson, M. E. Casida, C. Daul, A. Goursot, A. Koester, E. Proynov, A. St-Amant, D. R. Salahub, V. Carravetta, A. Duarte, N. Godbout, J. Guan, C. Jamorski, M. Leboeuf, M. Leetmaa, M. Nyberg, L. Pedocchi, F. Sim, L. Triguero, and A. Vela, StoBe-deMon (deMon Software, Stockholm-Berlin, 2005).
[31] L. Triguero, L. G. M. Pettersson, and H. Ågren, Phys. Rev. B **58**, 8097 (1998).
[32] W. Kutzelnigg, U. Fleischer, and M. Schindler, *NMR-Basic Principles and Progress* (Springer-Verlag, Heidelberg, 1990).
[33] L. G. M. Pettersson, U. Wahlgren, and O. Gropen, J. Chem. Phys. **86**, 2176 (1987).
[34] S. Huzinaga, J. Chem. Phys. **42**, 1293 (1965).
[35] C. Kolczewski, R. Püttner, O. Plashkevych, H. Ågren, V. Staemmler, M. Martins, G. Snell, A. S. Schlachter, M. Sant'Anna, G. Kaindl, and L. G. M. Pettersson, J. Chem. Phys. **115**, 6426 (2001).
[36] O. Takahashi and L. G. M. Pettersson, J. Chem. Phys. **121**, 10339 (2004).
[37] I. Bako, T. Megyes, and G. Palinkas, Chem. Phys. **316**, 235 (2005).
[38] S. Myneni, Y. Luo, L.-Å. Näslund, M. Cavalleri, L. Ojamäe, H. Ogasawara, A. Pelmenschikov, Ph. Wernet, P. Väterlein, C. Heske, Z. Hussain, L. G. M. Pettersson, and A. Nilsson, J. Phys.: Condens. Matter **14**, L213 (2002).
[39] R. Ludwig, Angew. Chem. Int. Ed. **40**, 1808 (2001).
[40] J. Stöhr, F. Sette, and A. L. Johnson, Phys. Rev. Lett. **53**, 1684 (1984).
[41] M. Odelius, M. Cavalleri, A. Nilsson, and L. G. M. Pettersson, Phys. Rev. B **73**, 024205 (2006).
[42] S. Paul and A. Chandra, J. Chem. Phys. **123**, 184706 (2005).
[43] I. Bako, T. Megyes, T. Grosz, G. Palinkas, and J. Dore, J. Mol. Liq. **125**, 174 (2006).
[44] D. Zhang, J. Gutow, K. B. Eisenthal, and T. F. Heinz, J. Chem. Phys. **98**, 5099 (1993).